J. Eng. Technol. Sci., Vol. 54, No. 4, 2022, 220408

Design of Split-Hopkinson Pressure Bar Specimen Fixture to Accommodate Punch and Double-Notch Shear Testing

Arya Dipajaya Nugraha, Kemal I. Ahmad & Muhammad A. Kariem*

Faculty of Mechanical and Aerospace Engineering, Institut Teknologi Bandung
Jalan Ganesa No. 10, Bandung, West Java 40132, Indonesia
*E-mail: kariem@itb.ac.id

Highlights:

- Split-Hopkinson shear bar testing can be conducted with a conventional solid transmission bar by employing the designed fixture.
- The double-notch specimen fixture provides great strain wave accuracy and force equilibrium conditions.
- The fixture length and transmission wall diameter were the two main design parameters in designing the SHSB double-notch fixture.
- The punch fixture still needs further development to decrease the time to attain force equilibrium.
- The mass of the fixture-transmission bar system and the diameter difference between fixture and transmission bar were the two main design parameters in designing the SHSB punch fixture.

Abstract. This study focused on the design of a specimen fixture which can be installed on the end of a conventional transmission bar so that shear testing (punch and double-notch) can be conducted with any conventional split-Hopkinson apparatus. The research was conducted by using the finite element method in Abaqus/CAE with 6061-T651 Aluminum as the specimen material. The research successfully determined the effect of the fixture's geometry and dimensions on the split-Hopkinson shear bar testing results. The optimum double-notch fixture provides great accuracy, having only a shear stress value difference of 1.49% with the original setup, while attaining force equilibrium after only 70 μs. The punch fixture, however, could only reach force equilibrium after 100 μs, thus providing too few observable data. Future work on the punch fixture is needed.

Keywords: *double-notch; fixture; impact; property; punch; shear; Split-Hopkinson bar.*

1 Introduction

The Kolsky bar, also widely known as the split-Hopkinson pressure bar (SHPB), is a device that was developed to obtain material properties in high-order strain rates from 10^2 to 10^4 s^{-1} [1]. In other words, the device can be used to acquire stress-strain curves for impact application. The device utilizes strain wave propagation, which enables us to acquire a specific data set for high-order strain rate application. Compared to conventional impact testing devices, the SHPB

Received May 27th, 2021, Revised December 17th, 2021, Accepted for publication March 25th, 2022.
 ISSN: 2337-5779,
DOI: 10.5614/j.eng.technol.sci.2022.54.4.8

offers two crucial advantages. The first one is the amount of detailed information that the device can acquire and the flexibility to control the loading conditions and parameters of the specimen [1].

A derivation of the SHPB is the split-Hopkinson shear bar (SHSB). The SHSB is a device that is used to acquire material responses under dynamic shearing load. The main difference between a conventional SHPB and an SHSB is the geometry of the testing specimen. The geometry of the specimen is paramount for obtaining results that are expected from either SHPB or SHSB tests [2]. There are three different specimen geometries that are normally used in SHSB testing: hat-shaped, punch, and double-notch [3-5].

Previous studies have been conducted to study the best performing SHSB techniques and specimen parameters. Budiwantoro, *et al.* [6] state that hat-shaped specimens are preferable, as they can be tested with a conventional solid transmission bar. For the punch and double-notch techniques, however, a hollow transmission bar is necessary. This leads to cost inefficiencies in production and application, since the transmission bar was designed for specific techniques, so it cannot be used for other techniques. On the other hand, Febrinawarta [7] states that optimized punch and double-notch specimens have certain advantages in terms of the generated shear stress-shear strain curve compared to hat-shaped specimens.

This paper discusses the possibility of using a specimen fixture that can be installed between the specimen (punch or double-notch) and a solid transmission bar. The idea is to eliminate the drawbacks of using a hollow transmission bar as in punch and double-notch testing. A similar approach has been conducted for a brittle specimen with the punch technique [8]. Further investigation is needed to apply it to a ductile specimen with the double-notch technique. The present research used the finite element method to simulate SHSB testing with several variants of the fixture installed. The results of the simulation were then validated theoretically and experimentally. The outcome of the research is the determination of the critical fixture design parameters and the optimum fixture for the punch and the double-notch technique respectively.

2 Description of Split-Hopkinson Shear Bar Technique

The transmission bar aside, the SHSB apparatus is similar to a conventional SHPB. It consists of four main components: striker bar, incident bar, specimen, and a hollow transmission bar. In order to use a conventional SHPB for conducting punch or double-notch testing, an additional specimen fixture is installed in between the specimen and the transmission bar. This fixture is basically a short hollow component to replace the main function of the hollow

transmission bar, which is to hold the specimen. Schematics of the apparatus for the modified punch and double-notch techniques are shown in Figure 1(a) and 1(b), respectively.

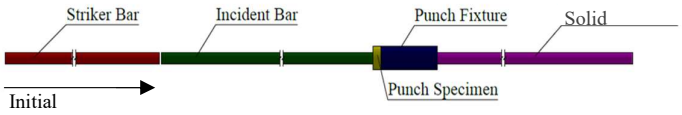

(a)

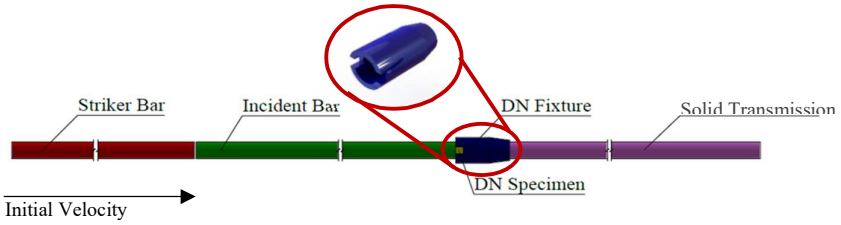

(b)

Figure 1 Construction schemes for the SHSB test (not at scale): (a) punch technique, (b) double-notch technique.

2.1 Fixture for Punch Testing

Three punch specimen fixtures were designed to study the effect of fixture length, fixture diameter and fixture-transmission bar total mass on the punch testing output. The geometry and dimensions of the punch fixtures are shown in Figure 2 and Table 1, respectively.

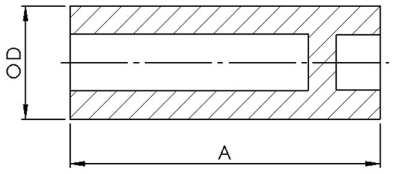

Figure 2 Geometry of punch fixtures.

Table 1 Dimensions of punch fixtures.

Parameters	Symbol	P1	P2	P3
Fixture Length	A	30 mm	100 mm	30 mm
Fixture Outer Diameter	OD	12.7 mm	22 mm	37.4 mm
Mass of Fixture and TB	m	0.32 kg	0.59 kg	0.59 kg

2.2 Fixture for Double-Notch Testing

Four double-notch specimens, fixtures were designed to study the effect of fixture length and fixture transmission wall diameter on the double-notch testing output. The geometry and dimensions of the double-notch fixtures are shown in Figure 3 and Table 2, respectively.

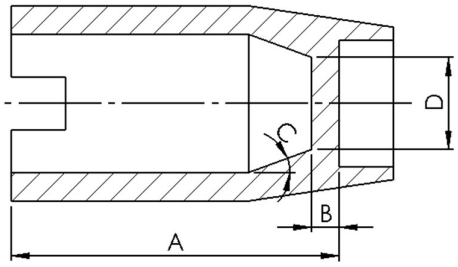

Figure 3 Geometry of double-notch fixtures.

Table 2 Dimensions of double-notch fixtures.

Parameters	Symbol	Unit	DN1	DN2	DN3	DN4
Fixture Length	A	mm	30	15	30	35
Wall Thickness	B	mm	2.5	2.5	2.5	2.5
Inner Diameter Angle	C	deg	20	20	20	20
Wall Diameter	D	mm	8.4	8.4	3	3

3 Loading, Data Processing, and Calculation Technique

Loading of the specimen is initiated by an impact of the striker bar and the incident bar. The initial velocity is given to the striker bar by a pneumatic gun. The impact generates a strain wave that propagates through the incident bar and the specimen to the transmission bar. The strain data needs to be classified as incident, reflected, and transmitted waves, as shown in Figure 4. Furthermore, Figure 5 shows a free body diagram of the specimen during SHSB testing.

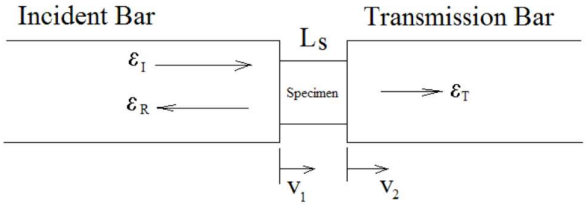

Figure 4 Incident strain, reflected strain, and transmitted strain on the incident and transmission bars.

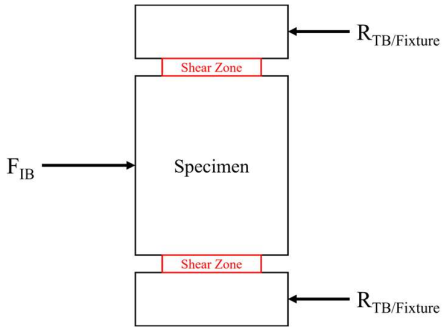

Figure 5 Free body diagram of a typical SHSB specimen.

Further data processing for these strain waves is needed to obtain a representative SHSB test result. The three strain waves are plotted in the same time frame to form an IRT (incident-reflected-transmitted) curve by using the Lifshitz and Leber method [9], as shown in Figure 6.

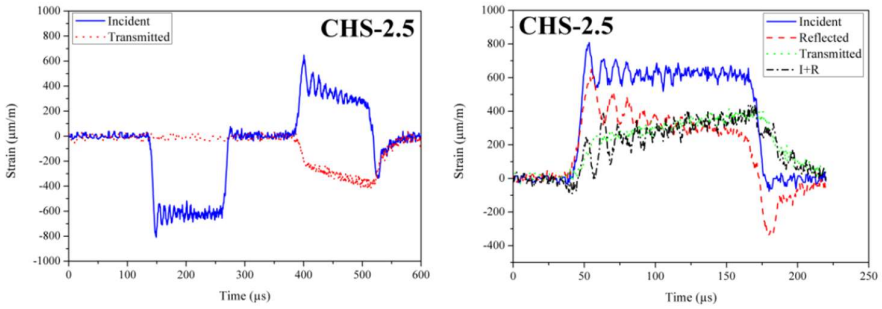

Figure 6 Typical strain wave from SHSB testing: (left) pre-processed from strain gauges and (right) post-processed IRT curve.

To convert the IRT curve into useful data, Eqs. (1) to (3) are employed to attain the values (as a function of time) of shear strain rate, shear strain, and shear stress, respectively [10].

$$\dot{\gamma}(t) = -2\frac{c_o}{L_S}(\varepsilon_R(t)) \tag{1}$$

$$\gamma(t) = -2\frac{c_o}{L_S}\left(\int_o^t \varepsilon_R(t)dt\right) \tag{2}$$

$$\tau(t) = \frac{A_{TB}}{A_S} E_{TB}\varepsilon_T(t)cos\theta \tag{3}$$

where $\dot{\gamma}$ is the shear strain rate, γ is the shear strain, τ is the shear stress, c_o is the wave velocity of the material, L_S is the specimen length, ε_R is the reflected wave,

A_{TB} is the transmission bar area, A_S is the shear area, E_{TB} is the transmission bar modulus of elasticity, ε_T is the transmitted strain, and θ is the shear angle. Figure 7 shows the punch and double-notch specimen geometries as well as the shear angle and shear zone to further demonstrate shear angle θ and shear area A_S in Eq. (3).

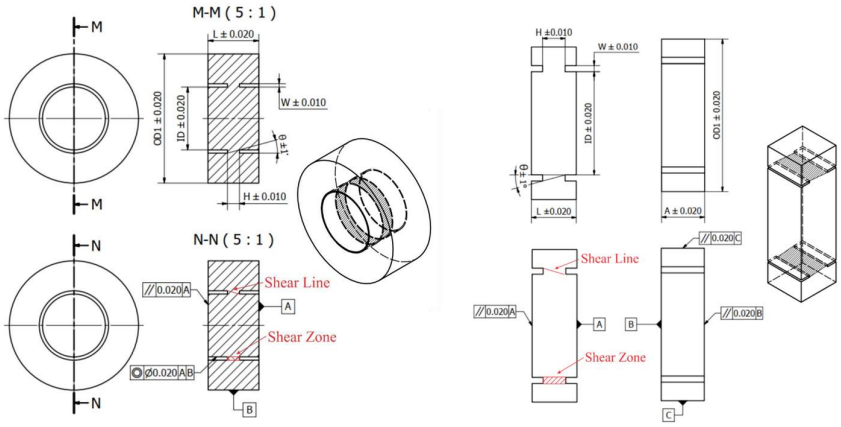

Figure 7 Schematic of: (left) punch specimen and (right) double-notch specimen.

4 Numerical Simulation and Validation

Seven finite element analyses, three for the punch technique (i.e., P1, P2, and P3) and four for the double-notch technique (i.e., DN1, DN1, DN3, and DN4) were conducted to study the effect of fixture dimensions and geometry on the result of the tests.

4.1 Data and Parameters

The apparatuses used in this research were based on the SHPB located in Swinburne University of Technology, Australia. While the fixtures are additional components, as explained in Section 3, the striker bar, pressure bar, and specimen were based on the existing SHPB and will discussed in the following subsection.

4.1.1 Striker Bar, Incident Bar and Transmission Bar

The dimensions of the striker bar, incident bar, and transmission bar were taken from Ref. [11] and are shown in Table 3. Maraging steel (AISI Grade 18Ni) was the material used for the striker bar, incident bar, transmission bar, and fixture. The mechanical properties of maraging steel are shown in Table 4 [12].

Table 3 Dimensions of the bars [11].

Technique	Bar Type	Inner Diameter (mm)	Outer Diameter (mm)	Length (mm)
Striker Bar (SB)				
Punch	Solid	-	6.18	300
Double-notch	Solid	-	11.50	300
Incident Bar (IB)				
Punch	Solid	-	6.18	1,200
Double-notch	Solid	-	11.50	1,200
Hollow Transmission Bar (TB)				
Punch	Hollow	6.40	12.70	1,200
Double-notch	Hollow	12.60	17.80	1,200
Solid Transmission Bar (TB)				
Punch	Solid	-	6.18	1,200
Double-notch	Solid	-	11.50	1,200

Table 4 Properties of maraging steel [12].

Properties	Symbol	Value	Unit
Density	ρ	8070.2	kg/m^3
Modulus of Elasticity	E	185.94	GPa
Bar Wave Velocity	c_0	4800	m/s
Poisson's Ratio	v	0.307	-

4.1.2 Specimen

The material used for the specimen was 6061-T651 Aluminum. The constitutive Johnson-Cook equation was used. The elastic properties used were taken from Ref. [13] and are listed in Table 5, while the Johnson-Cook plasticity model and Johnson-Cook damage parameter were taken from Ref. [7] and are listed in Tables 6 and 7 respectively.

Table 5 6061-T651 Aluminum elastic properties [13].

Properties	Symbol	Value	Unit
Density	ρ	2700	kg/m^3
Modulus of Elasticity	E	68.9	GPa
Bar Wave Velocity	c_0	0.33	-
Shear Modulus	G	26.0	GPa
Poisson's Ratio	v	5051.6	m/s

Table 6 Johnson-Cook plasticity parameters for 6061-T651 Aluminum [7].

Parameter	Symbol	Value	Unit
True Yield Strength	A	360.23	MPa
Strain Hardening Constant	B	802.62	MPa
Strain Hardening Exponent	n	0.923	-
Strain Rate Coefficient	C	1 x 10^{-8}	s^{-1}
Thermal Softening Exponent	m	1	-
Melting Temperature	T_{melt}	925	K
Room Temperature	T_{room}	294	K

Table 7 Johnson-Cook Damage parameters for 6061-T651 Aluminum [7].

Parameter	Symbol	Value	Unit
Initial Failure Strain	D_1	- 0.77	-
Exponential Factor	D_2	1.45	-
Triaxiality Factor	D_3	- 0.45	-
Strain Rate Factor	D_4	0	-
Temperature Factor	D_5	1.60	-
Melting Temperature	T_{melt}	925	K
Room Temperature	T_{room}	294	K

As for the geometry and dimensions, for each of the techniques different design parameters were used. These are provided in Figure 4 and the values are shown in Table 8 for the punch specimen and Table 9 for the double-notch specimen.

Table 8 Punch specimen parameters [7].

Parameter	Value	Unit
Shear Angle (θ)	4.99	Degree (°)
Shear Area	24.99	mm^2
OD 1	12.70	mm
ID	6.18	mm
W	0.11	mm
H	1.26	mm
L	5.00	mm

Table 9 Double-notch specimen parameters [7].

Parameter	Value	Unit
Shear Angle (θ)	5.07	Degree (°)
Shear Area	24.96	mm^2
OD 1	17.00	mm
ID	11.50	mm
W	0.23	mm
H	2.59	mm
L	5.00	mm
A	4.80	mm

4.1.3 Velocity of Striker Bar

The initial velocity of the striker bar was varied for each technique due to the difference in diameter of the striker bar. These variations were set so that the kinetic energy of each technique would be relatively the same and high enough to generate a minimum strain of 10%. The striker bar's initial velocities for the different techniques were taken from Ref. [14] and are listed in Table 10.

Table 10 Striker bar initial velocity for each technique [14].

Apparatus	Technique	Diameter (mm)	Length (mm)	Velocity (m/s)	Kinetic Energy (Joule)
SUT	Punch	6.18	300	14.215	7.337
	Double Notch	11.50	300	7.639	7.337

4.2 Finite Element Modelling

The finite element model in this research used a 3D symmetrical quarter of the real apparatus, with the X-axis set as the main axis. The symmetry planes for the model were plane XY and plane ZX. A 3D symmetrical quarter model was employed to reduce the time required to complete the simulation. The components, i.e., striker bar, incident bar, specimen, fixture and transmission bar, were 3D modeled in Solidwork and then imported to Abaqus/CAE to be modeled as finite elements. Abaqus/CAE was used due its ability to generate finite element models with dynamic loading conditions. A hexagonal element type was employed for all components.

A global seed size of 1 mm was used for the striker bar, incident bar and transmission bar, while 0.5 mm and 0.1 mm seeds were used for the fixture and the specimen, respectively. The type of simulation used was dynamic explicit with a duration of 600 μs and an output data frequency of 2 MHz. The meshing output of the components is shown in Figure 8.

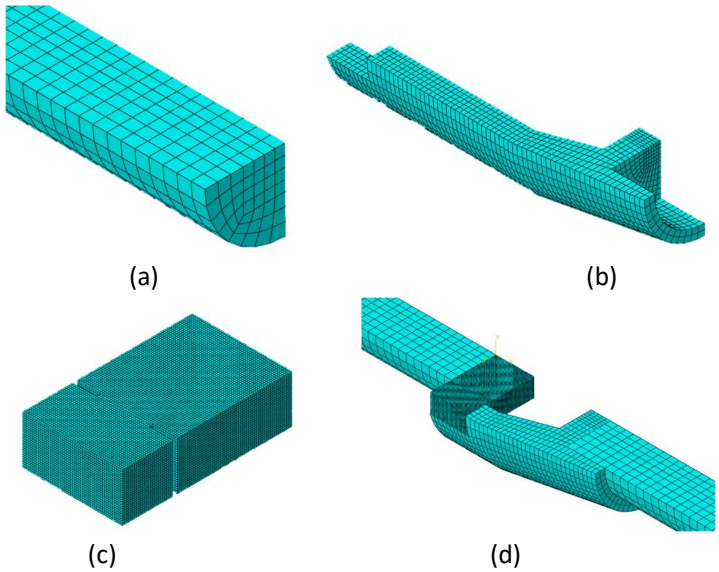

Figure 8 Finite element model (not at scale) of (a) bars, (b) fixture, (c) specimen, (d) assembly of the SHSB apparatus.

4.3 Validation of Finite Element Model

To ensure that the simulations conducted in this research would provide reliable results, validation of the finite element model was conducted. Two validations

were conducted, i.e., validation of the elastic wave propagation and validation of the plastic stress value.

4.3.1 Validation of Elastic Wave Propagation

Validation of the elastic wave propagation was carried out theoretically by comparing the average value of the incident wave strain. The average value of the incident wave strain generated from the simulation was 2214.5 με and is shown in Figure 9.

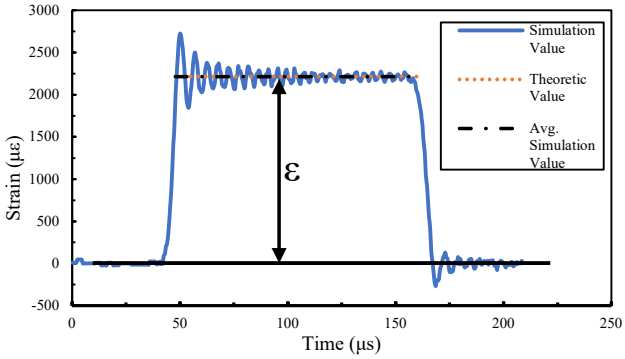

Figure 9 Comparison of theoretical and simulation generated incident wave.

By using the one-dimensional wave propagation theorem, Eq. (4) was developed to obtain the theoretical incident strain value, which was 2215 με.

$$\varepsilon = \frac{V_{SB}}{2\sqrt{\frac{E}{\rho}}} = \frac{22.642}{2\sqrt{\frac{185.94}{8070.2}}} = 2215\ \mu\varepsilon \tag{4}$$

Thus, the error between the simulated and theoretical values was 0.022%. Since the error is below 1%, the simulation was deemed valid.

4.3.2 Validation of Plastic Stress Value

Validation of the plastic stress value was carried out experimentally by comparing the simulation result to the experimental result conducted by Febriawarta [7]. The strain data from the experiment and the numerical analysis were processed in accordance with Section 3.

The stress-strain data obtained from the experiment is shown on Table 11. The value difference with the true stress-true strain curve was then assessed after the ringing-up period, as explained by Chen and Song [1], ranging from 0.078ε to 0.144ε. Based on the comparison shown in Figure 10, the difference was 3.90%

and thus the simulation was deemed valid, as the difference was below the 5% threshold.

Table 11 Experiment stress-strain data [7].

ε	σ (MPa)	ε	σ (MPa)	ε	σ (MPa)
0.000	46.687	0.156	577.875	0.205	102.345
0.011	244.780	0.168	607.230	0.211	102.114
0.031	336.391	0.179	612.192	0.216	-11.772
0.055	392.798	0.185	629.686	0.217	-210.821
0.079	457.787	0.184	429.377	0.211	-296.647
0.100	491.962	0.183	161.552	0.206	0.000
0.118	513.401	0.187	137.260	0.206	0.000
0.132	555.371	0.193	104.958	0.206	0.000
0.144	578.652	0.198	83.329	0.206	0.000

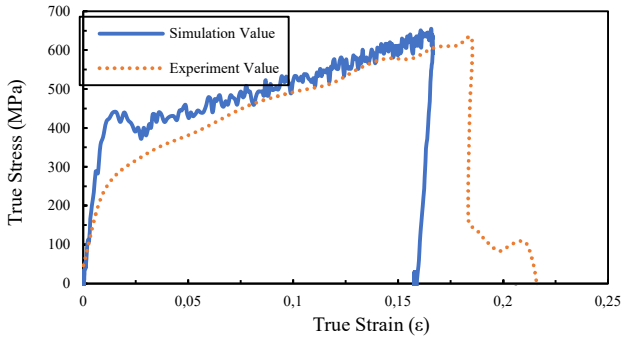

Figure 10 Comparison of true stress-true strain curve generated in the simulation and the experiment.

Before 0.078ε, there were notable differences in the true stress value. Two factors are of interest: the ringing-up period and the number of data available from the experiment. The ringing-up period, or 'unreliable region', as it is called by Kariem [10], is the period during which the steady state condition has yet to be attained by the system. This phenomenon causes the occurrence of stress fluctuation at the beginning of the stress-strain curve. In this case, however, only four data points were available before the steady state condition, as shown in Table 11. Thus, the fluctuation could not be captured, so it seems like there was a gap between the experimental and the simulation value. Nonetheless, as the name suggests, data from the 'unreliable region' should not be used for engineering purposes.

The second observable phenomenon was that both curves did not share the same final strain value. As mentioned by Kariem [10], this phenomenon is also

tolerable, because the final strain value is not important for application. Furthermore, the difference is caused by inevitable factors in the experiment, such as gravity, friction, and pressure drop in the loading gun, affecting the velocity in the system. Thus, the phenomenon is negligible in the case of experimental validation of a finite element model.

5 Results and Discussion

The finite element analysis results were then interpreted to determine the best fixture for the punch and double-notch techniques. Typical shear stress distributions of both specimens are shown in Figure 12. The best fixture was then determined by two parameters, i.e., the time required to attain force equilibrium of each fixture, and the plastic stress value difference compared to a normal SHSB setup (with hollow transmission bar). Also, the crucial design parameters of the fixture geometry were determined by analyzing the simulation results.

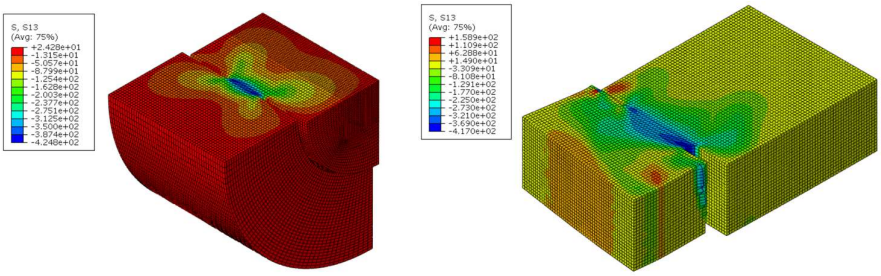

Figure 11 Shear stress distribution of (left) punch specimen and (right) double-notch specimen.

5.1 Punch Fixture

The conventional hollow transmission bar had a mass of 0.59 kg, while the modified solid transmission bar, which was identical to the incident bar, had a mass of only 0.29 kg. This significant mass difference proved to influence the testing output, as the reflected wave of P1 was close to zero, while the transmitted wave was notably higher compared to the normal punch transmitted curve, as shown in Figures 12 and 13, respectively. The reflected waves of P2 and P3, however, show a close resemblance to the normal punch reflected curve, since the fixture-transmission bar system had a total mass of 0.59 kg. Even though the reflected waves were corrected, the transmitted waves still differed compared to the normal punch. The large cross-sectional area of the punch, which was designed to compensate for its lower mass, resulted in a longer time to transfer all strain waves.

The best fixture for the punch technique was selected by comparing the time needed to reach force equilibrium. P1 reached force equilibrium after 100 μs, while P2 and P3 both reached force equilibrium after 150 μs, as shown in Figure 14. Thus, P1 was selected as the best fixture for the punch technique. However, this resulted in a lack of usable data, as the stress-strain curve could only be utilized after force equilibrium was attained. Thus, future work is required for the punch fixture to be applied for testing.

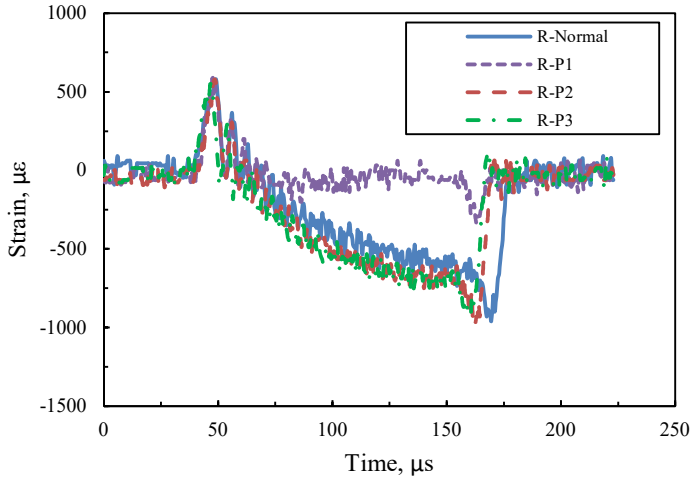

Figure 12 Reflected wave comparison of punch fixtures.

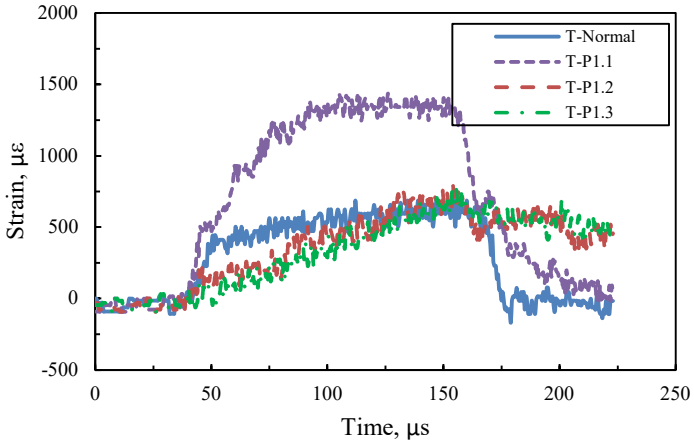

Figure 13 Transmitted wave comparison of punch fixtures.

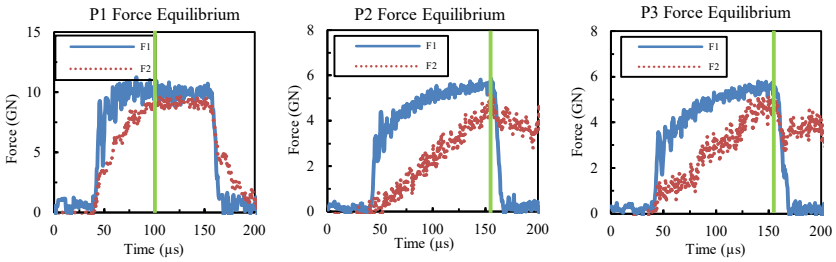

Figure 14 Force equilibrium of P1, P2, and P3.

5.2 Double-Notch Fixture

Force equilibriums for all double-notch fixtures were attained after only 70 µs. The value shows that the majority of the data could be utilized for engineering use. The force equilibrium of the three models is provided in Figure 15.

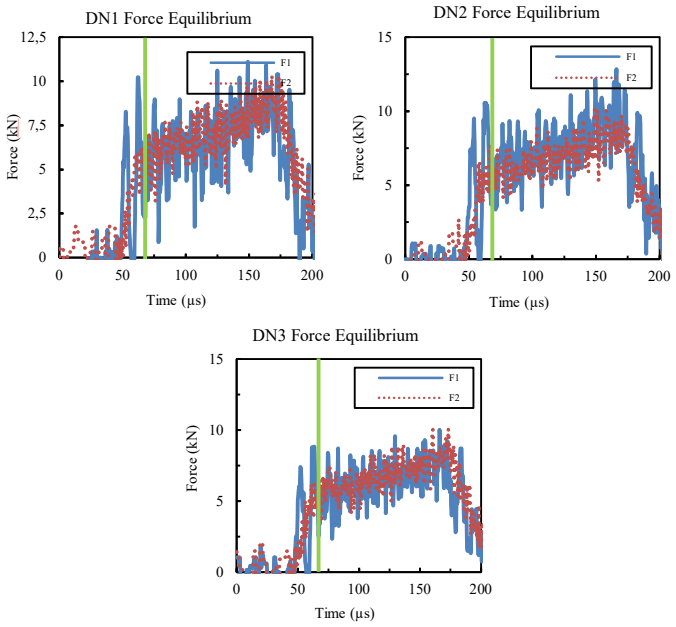

Figure 15 Force equilibrium of DN1, DN2, and DN3.

Yet, it is noticeable that the oscillation was greater in the double-notch specimen compared to the punch specimen. The reason is that, as shown in Figure 16, the deformed double-notch specimen (shown on the left) tended to hit

the side of the incident bar, unlike the punch specimen, resulting in an additional strain wave captured by the strain gage. The fact that the oscillations of F1, which represents the wave measured in the incident bar, were far greater than those of F2, gives more evidence of this phenomenon. Nonetheless, the matter is trivial considering the fact that only the average value will be of use for most applications. Thus, true stress-true strain curves for DN1, DN2, and DN3 were generated, as shown in Figure 17.

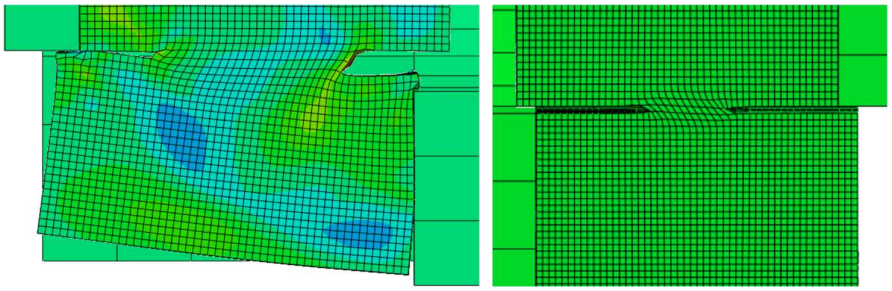

Figure 16 Comparison of double-notch specimen (left) and punch specimen (right) after SHSB testing.

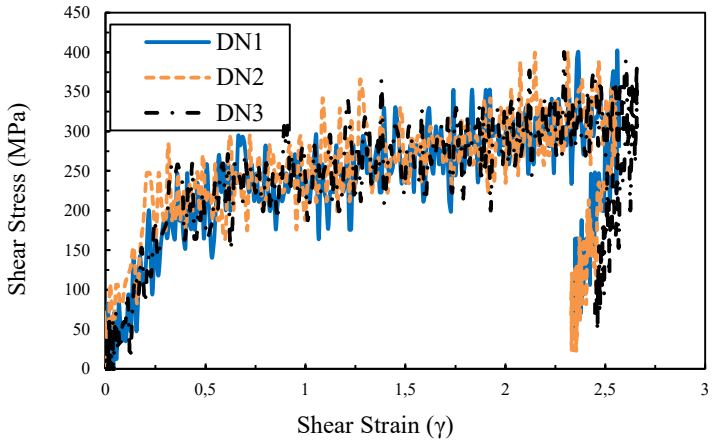

Figure 17 Shear stress-shear strain curve comparison of DN1, DN2, and DN3.

Trendline equations of the plastic area for DN1, DN2 and DN3 were generated through linear regression to demonstrate the effect of fixture length and fixture transmission wall diameter on the testing output. DN2, which is identical to DN1 with a modified length, showed a change in its curve constant, while maintaining the gradient. DN3, which is identical to DN1 with a modified transmission wall

diameter, showed a change in the gradient, while maintaining the curve constant. The trend line equations of shear strain, in MPa, as the function of shear strain for DN1, DN2 and DN3, are given by Eqs. (5), (6), and (7).

$$\tau = 48.732\gamma + 192.79 \quad (5)$$

$$\tau = 48.815\gamma + 199.04 \quad (6)$$

$$\tau = 53.654\gamma + 191.74 \quad (7)$$

DN4 was the best fixture for the double-notch technique, with its optimized length and transmission wall diameter value. Force equilibrium was attained after 70 µs, as shown in Figure 18. The true stress-true strain curve was then created to be compared with the normal SHSB double-notch true stress-true strain curve, as shown in Figure 19. Both curves have a close resemblance, demonstrating that installing DN4 on the SHSB double-notch apparatus generated a negligible disturbance. The error value of the average true stress was relatively small, 1.49%, across the plastic area.

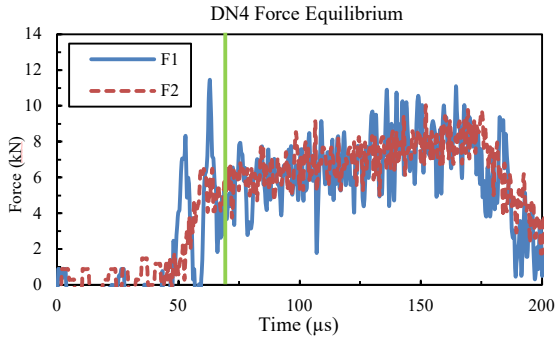

Figure 18 Force equilibrium of DN4.

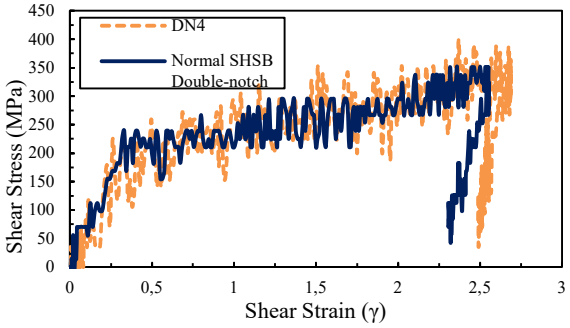

Figure 19 Shear stress-shear strain curve of DN4 and normal SHSB DN.

6 Conclusion

Valid assumptions were achieved for all finite element analyses. This shows that conversion of a conventional Split-Hopkinson bar to accommodate shear testing by using an additional fixture can be conducted. The results, however, will be further be validated by conducting lab-scale testing.

The best punch fixture was P1 with force equilibrium reached after 100 μs, while the others took 50 μs longer. The system mass and cross-sectional area difference between the fixture and the transmission bar were the main design parameters in designing the punch fixture. The above factors contributed to a long time to reach force equilibrium, leaving too little useful data to be processed. Thus, future work is required to further develop the punch fixture for application.

The best double-notch fixture was DN4, with a difference of 1.49% compared to the normal double-notch testing result. A conclusion that can be drawn from this research is that for the double-notch fixture, the length of the fixture has a notable effect on the true stress-true strain curve intersection with the y-axis, while the fixture transmission wall diameter affects the gradient of the curve. The double-notch fixture is ready for application, since it provides excellent accuracy and force equilibrium.

Acknowledgement

This work was carried out at the Engineering Design Laboratory, Mechanical Engineering Department, Faculty of Mechanical and Aerospace Engineering, Institut Teknologi Bandung and was financially supported by Institut Teknologi Bandung through P2MI (*Penelitian Pengabdian Masyarakat dan Inovasi*).

References

[1] Chen, W. & Song, B., *Split Hopkinson (Kolsky) Bar: Design*, Testing and Applications, Springer, New York, 2011.

[2] Pankow, M., *Specimen Size and Shape Effect in Split Hopkinson Pressure Bar Testing*, University of Michigan, Michigan, 2009.

[3] Schwer, L.E., *Aluminum Plate Perforation: A Comparative Case Study using Lagrange with Erosion, Multi-material Ale, and Smooth Particle Hydrodynamics*, in 7th European LS-DYNA Conference, Salzburg, 2009.

[4] Peirs, J., Verleysen, P., Degrieck, J. & Coghe, F., *The Use of Hat-shaped Specimens to Study the High Strain Rate Shear Behavior of Ti-6Al-4V*, International Journal of Impact Engineering, **37**, pp. 703-714, 2010.

[5] Dowling, A.R. *The Dynamic Punching of Metals*, Journal of Institute of Metals, **98**, pp. 215-224, 1970.

[6] Budiwantoro, B., *Results Comparison for Hat-shaped, Double-notch and Punch Testing of Split Hopkinson Shear Bar Technique*, J. Eng. Technol. Sci., **51**(6), pp. 805-823, 2019.

[7] Febrinawarta, B., *A Finite Element Study on Three Methods of Split Hopkinson Shear Bar Testing,* Master Thesis, Mechanical Engineering, Faculty of Mechanical and Aerospace Engineering, Institut Teknologi Bandung, Bandung, Indonesia, 2019.

[8] Huang, S., Tiang Feng, X. & Xia, K., *A Dynamic Punch Method to Quantify the Dynamic Shear Strength of Brittle Solids*, The Review of Scientific Instruments, **82**(5), 053901, 2011.

[9] Lifshitz, J.M. & Leber, H., *Data Processing in the Split Hopkinson Pressure Bar Tests*, International Journal of Impact Engineering, **15**, pp. 723-733, 1994.

[10] Kariem, M.A., *Reliable Materials Performance Data from Impact Testing*, Doctor of Philosophy, Faculty of Engineering and Industrial Sciences, Swinburne University of Technology, Hawthorn, 2012.

[11] Kariem, M.A., Santiago, R.C., Govender, R., Shu, D.W. Ruan, D., Nurick, G., Alves, M., Lu, G. & Langdon, G.S., *Round-Robin Test of Split Hopkinson Pressure Bar*, International Journal of Impact Engineering, **126**, pp. 62-75, 2019.

[12] Kariem, M.A & Ruan, D., *Improving the Split-Hopkinson Pressure Bar Testing Tech*, 2017.

[13] MATWEB Material Property Data, *Aluminum 6061-T6; 6061-T651*, 2019. http://matweb.com/search/DataSheet.aspx?MatGUID=b8d536e0b9b54bd7b69e4124d8f1d20a&ckck=1. (9 February 2019)

[14] Edwards, N.J., Kariem, M.A., Rashid, R.A.R., Cimpoeru, S.J., Lu, G. & Ruan D., *Dynamic Shear Testing of 2024 T351 Aluminium at Elevated Temperature*, Materials Science and Engineering: A, **754**, pp. 99-111, 2019.